

# Rapid surface texturing to achieve robust superhydrophobicity, controllable droplet impact, and anti-frosting performances

Qingwen DAI<sup>1,\*</sup>, Lei CHEN<sup>1</sup>, Jiabao PAN<sup>3</sup>, Liping SHI<sup>4</sup>, Dameng LIU<sup>2,\*</sup>, Wei HUANG<sup>1</sup>, Xiaolei WANG<sup>1</sup>

<sup>1</sup> College of Mechanical and Electrical Engineering, Nanjing University of Aeronautics & Astronautics, Nanjing 210016, China

<sup>2</sup> State Key Laboratory of Tribology in Advanced Equipment, Department of Mechanical Engineering, Tsinghua University, Beijing 100084, China

<sup>3</sup> School of Mechanical Engineering, Anhui Polytechnic University, Wuhu 241000, China

<sup>4</sup> School of Mechanical Engineering, Anhui University of Technology, Ma'anshan 243032, China

Received: 12 April 2022 / Revised: 13 February 2023 / Accepted: 08 March 2023

© The author(s) 2023.

**Abstract:** Robust superhydrophobic surfaces with excellent capacities of repelling water and anti-frosting are of importance for many mechanical components. In this work, wear-resistant superhydrophobic surfaces were fabricated by curing a mixture of polyurethane acrylate (PUA) coating and 1H,1H,2H,2H-Perfluorodecyltrichlorosilane (HFTCS) on titanium alloy (TC4) surfaces decorated with micropillars pattern, thus, composite functional surfaces with PUA coating in the valleys around the micropillars pattern of TC4 were achieved. Apparent contact angle on fabricated surfaces could reach 167°. Influences of the geometric parameters of micropillars pattern on the apparent contact angle were investigated, and the corresponding wear-resistant property was compared. Droplet impact and anti-frosting performances on the prepared surfaces were highlighted. An optimized design of surface texture with robust superhydrophobicity, controllable droplet impact, and anti-frosting performances was proposed. This design principle is of promising prospects for fabricating superhydrophobic surfaces in traditional mechanical systems.

**Keywords:** surface texture; robust superhydrophobic; wear-resistant; droplet impact; anti-frosting

## 1 Introduction

Since Young's equation was firstly introduced in 1805, wetting and wettability phenomena at the surface/interface maintain a research hotspot in which chemistry, physics, and engineering intersect [1–8]. Extreme wetting properties, especially superhydrophobicity, have wide applications in self-cleaning [9–12], anti-frosting or icing [13–15], directional transportation [16–18], and condensation heat transfer [19–21]. Inspired by natural surfaces such as lotus leaf, micro/nano structured surfaces with unique superhydrophobic properties had been successfully fabricated via techniques such as laser etching [22–25], chemical or electrochemical reaction [26–28], sol-gel

method [29–31], and thermal treatment [32]. Generally, superhydrophobic surfaces can be achieved by the means of low surface energy coatings or hierarchical micro/nano structures, of which the well-known Wenzel and Cassie–Baxter equations explain the mechanism to create a high contact angle [33–35].

The Cassie–Baxter regime represents a superhydrophobic state that a liquid droplet is unable to penetrate the valleys between the peaks on a micro structured surface and then the air is trapped beneath the droplet. Wenzel regime represents a state that a liquid droplet penetrates the micro valleys completely [36, 37]. To generate a stable Cassie–Baxter state, micro structures are always accompanied by nano structures to ensure the capillary pressure

\* Corresponding authors: Qingwen DAI, E-mail: daiqingwen@nuaa.edu.cn; Dameng LIU, E-mail: ldm@tsinghua.edu.cn

exceeds wetting pressure, enhancing the water-repellent performance [38–40]. With the assistance of hierarchical structures, Liu and Kim [41] fabricated superhydrophobic surfaces even for completely wetting liquids.

In general, micro/nano structures are of poor mechanical stability, maintaining superhydrophobicity and mechanical stability is vital for many applications, such as tribological interfaces where friction and lubrication both are influenced by contact angles [42] or biotechnology surfaces where self-cleaning and avoid-biofouling are required [43]. Over the past decades, a mass of studies was carried out to strengthen the micro/nano structures to maintain the superhydrophobic property. Strategies like optimizing the geometric morphology of microstructures [44, 45], replacing the nano structures with stable nanoparticles [46–48], and employing specific glue or crosslinker to reinforce the microstructures [49, 50], are all possible manners to maintain the superhydrophobic property, while some of them are at the expense of complex fabrication process or strong dependency of parameters. Recently, Wang et al. [51] reported a design principle to create robust superhydrophobicity via structuring microstructures as an interconnected surface frame containing pockets that house highly water-repellent and mechanically fragile nanostructures. Different from traditional methods that superhydrophobicity relies on the combined action of micro and nano structures, this research proposed a new approach that adopts microstructures and nanostructures to provide durability and water repellency, respectively.

Inspired by that, here, we proposed a rapid method to fabricate robust superhydrophobic surfaces. Decorating titanium alloy surfaces with micropillars pattern, and coating the valleys around the pattern with a mixture of polyurethane acrylate and 1H,1H,2H,2H-Perfluorodecyltrichlorosilane, superhydrophobicity property was achieved. Micropillars patterns with different geometric parameters were fabricated, and the corresponding superhydrophobic and wear-resistant properties were investigated. The wetting state and the wear-resistant mechanism was revealed. Droplet impact and anti-frosting performances on the designed surfaces were confirmed, and an optimized design of the surface texture with robust superhydrophobicity, controllable droplet impact, and anti-frosting performances was suggested.

## 2 Materials and methods

### 2.1 Materials

The substrates were made of titanium alloy (TC4, Ti–6Al–4V, Nanjing Iron and Steel Corporation, China) with a dimension of 20 mm in diameter and 3 mm in thickness. TC4 has favorable high strength, excellent corrosion, and heat resistance, which is widely used in aerospace. Making its surface with robust superhydrophobicity and excellent characteristics of repelling water and anti-frosting has promising prospects.

A typical light-curing resin, polyurethane acrylate (PUA, product number: CN996), was adopted for surface coating; the reactive diluent (Isobornyl methacrylate,  $C_{14}H_{22}O_2$ ) and photoinitiator (1-hydroxy-cyclohexyl phenyl ketone,  $C_{13}H_{16}O_2$ ) were necessary components for ultraviolet curing, and these reagents were purchased from Sartomer, USA. A low surface energy material, 1H,1H,2H,2H-Perfluorodecyltrichlorosilane (HFTCS,  $C_{10}H_4Cl_3F_{17}S$ , Aladdin, China) was adopted for surface modification. All chemicals were analytically pure and used as received.

### 2.2 Fabrication

TC4 surfaces were polished via sandpapers to an average surface roughness of  $\sim 0.2 \mu\text{m}$ . The surfaces were cleaned with ethanol, deionized water, and blow-dried with nitrogen. A basic PUA mixture was prepared by blending 61.4 wt%, 16 wt% isobornyl methacrylate, 2.4 wt% 1-hydroxy-cyclohexyl phenyl ketone PUA, and 20 wt% HFTCS together. Curing this PUA mixture on TC4 surfaces via UV-light, the superhydrophobic property was obtained. The apparent contact angle on the surface was approximately  $156^\circ$ . Basic properties of PUA coatings with different HFTCS contents are provided in Fig. S1 in the Electronic Supplementary Material (ESM)). Primary experiments indicated that this superhydrophobic coating was fragile and highly susceptible to abrasion when experiencing an external mechanical load and relative motion. To overcome this limitation, a type of wear-resistant superhydrophobic surface was designed in the following section and a constant content of 20 wt% HFTCS was adopted.



The detailed fabrication process is shown in Fig. 1(a). First, micropillars pattern was milled on a smooth TC4 surface via nanosecond laser treatment (KY-M-UV3L, Wuhan Keyi, China), and the parameter set for fabrication was similar to our previous work [52], of which the output power, scanning rate, and pulse width was 3 W, 50 mm/s, and 0.1  $\mu$ s, respectively. The normal processing time is approximately 30 min. Second, the PUA mixture was coated on the surface via a spin coating process with an initial rotational speed of 1,000 rpm for 30 s and a second rotational speed of 3,000 rpm for 30 s. The surface was then exposed to ultraviolet light (400 W, 2 min) for curing, and polished with sandpaper (2,000 mesh) under a very light hand pressure.

Figure 1(b) shows the progressively enlarged scanning electron microscopy (SEM) images of a

prepared surface with a parameter of  $L = 300 \mu\text{m}$  and  $r = 64\%$ , where  $L$  and  $r$  denotes the edge length of the pillar and the area ratio of PUA coating, respectively (the area ratio is calculated by:  $r = 1 - \frac{L^2}{(L+S)^2}$ , where

$\Delta S$  is the distance between two adjacent pillars). Micro square pillars pattern was formed on the TC4 surface, and PUA coating was cured in the surrounding valleys. The energy dispersive spectrometer (EDS) results indicate that most PUA coating on the metal support positions was removed, only with a little residuum (Fig. S2 in the ESM). Note that the lifetime of superhydrophobicity is important [53], thus, the apparent contact angle on this surface with elapsed time is confirmed. As shown in Fig. 1(c), the initial apparent contact angle on this surface is as high as  $167^\circ$  and it degrades over time, which is approximately

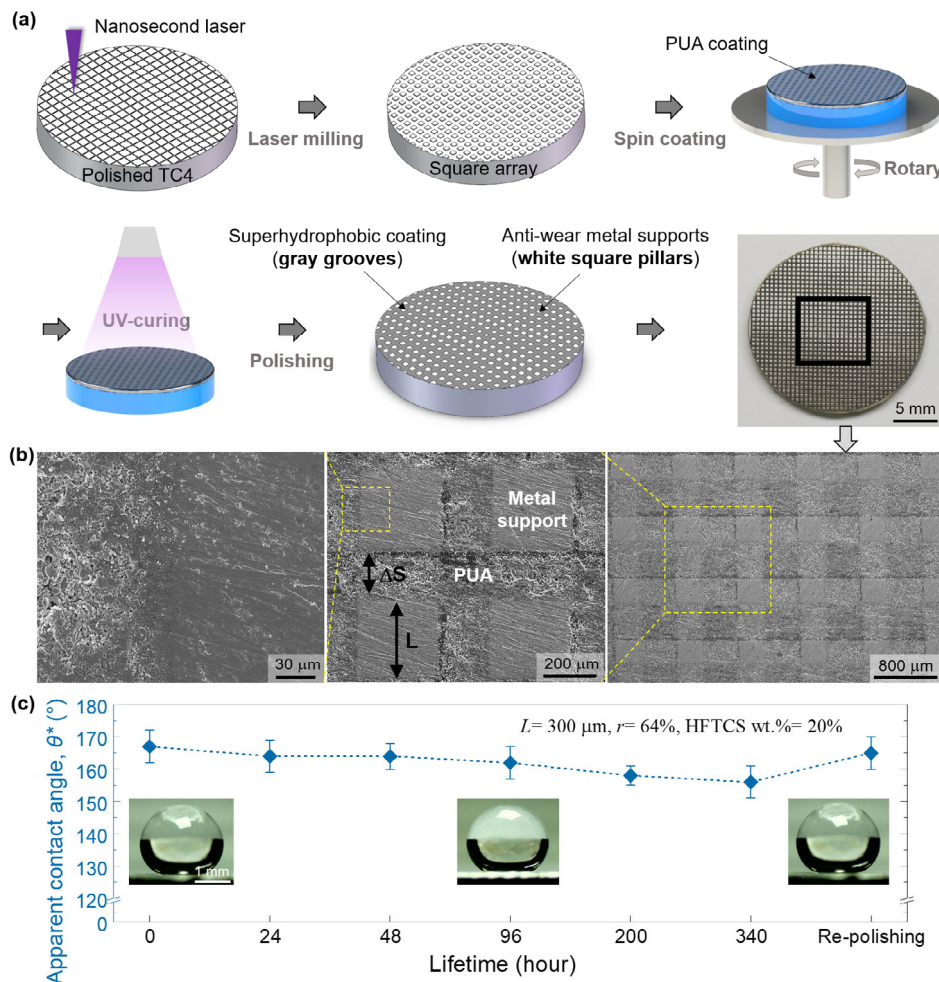


**Fig. 1** (a) Fabrication process of superhydrophobic surfaces of laser milling, spin coating, UV-curing, and polishing. (b) Progressively enlarged SEM images of a prepared surface. (c) Apparent contact angle on the prepared surface with elapsed time.

155° after 2 weeks. Re-polishing (2,000 mesh) this surface slightly to remove the adsorbed impurities from the air, the apparent contact angle returns to 166°. Table 1 lists the geometric parameters of the fabricated surfaces. Degradation of superhydrophobicity on these surfaces is approximately 10° for 2 weeks, and they all can back to the initial superhydrophobicity again via a re-polishing process.

### 2.3 Characterization

The apparent contact angle and roll-off angle was measured via a contact angle measuring instrument (SL-200B, Solon, China). Micro morphology and optical topography of the surfaces were measured via a SEM (JSM-6480LV, JEOL, Japan), a digital microscope

(VHX-600E, Keyence, Japan), and an atomic force microscope (Icon AFM, Bruker, USA). Droplet impact process was recorded via a high-speed camera (i-SPEED 726R, iX Cameras, UK). Anti-frosting property was investigated via a self-made apparatus, of which the frost mass was measured via a precision electronic balance (JB5374-91, Mettler Toledo, Switzerland). The dynamic process was captured by a digital camera (D750, Nikon, Japan) and a digital microscope, more detailed information about this experimental apparatus is provided in Fig. S3 in the ESM.

## 3 Results and discussion

### 3.1 Superhydrophobicity

All the prepared surfaces are superhydrophobic and the roll-off angles are relatively small. As shown in Fig. 2(a), when the area ratio is constant ( $r = 75\%$ ), the apparent contact angle on the surface with  $L = 100 \mu\text{m}$  is 151°, and it increases to 164° when  $L = 300 \mu\text{m}$ , as  $L$  further increases to  $500 \mu\text{m}$ , the apparent contact angle decreases slightly to 158°. For the roll-off angle, it decreases gradually from 3.7° to 2.6° when  $L$  increases from 100 to  $500 \mu\text{m}$ . As shown in Fig. 2(b), when the edge length is constant ( $L = 300 \mu\text{m}$ ), the apparent contact angle and the roll-off angle increase

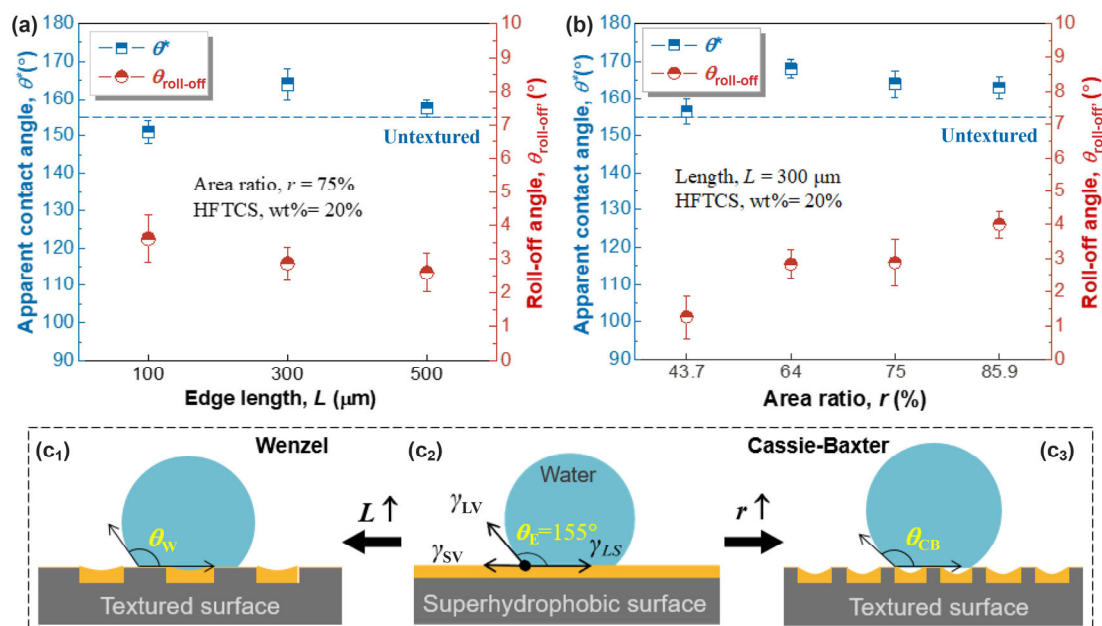


**Fig. 2** Influences of (a) the area ratio of PUA coating and (b) the edge length of the pillar on the apparent contact angle and the roll-off angle. (c) Schematic diagram of the wetting state of droplets on different surfaces.

gradually with increasing area ratio. One exception is that for the area ratio of 64%, the contact angle is approximately 167°.

The influence of micropillars on the wetting state is discussed as follows. Young equation describes the ideal equilibrium contact angle ( $\theta_E$ ) of a droplet on a solid surface (Fig. 2(c<sub>2</sub>)):

$$\cos \theta_E = \frac{\gamma_{SV} - \gamma_{SL}}{\gamma_{LV}} \quad (1)$$

where  $\gamma_{SV}$ ,  $\gamma_{SL}$ , and  $\gamma_{LV}$  denote the solid/vapor, solid/liquid, and liquid/vapor surface tension, respectively. When the surfaces become rough, the apparent contact angle can be evaluated via the Wenzel and Cassie–Baxter equations [54].

If a liquid can completely penetrate the micro valleys (Wenzel state, Fig. 2(c<sub>1</sub>)), the apparent contact angle ( $\theta_W$ ) can be expressed as

$$\cos \theta_W = r \cos \theta_E \quad (2)$$

where  $r$  is the ratio of the real to the projected area covered by the liquid.

If a liquid is unable to penetrate the valleys between the peaks on a micro structured surface and the air is trapped beneath it (Cassie–Baxter state, Fig. 2(c<sub>3</sub>)), the apparent contact angle ( $\theta_{CB}$ ) can be expressed as

$$\cos \theta_{CB} = f(\cos \theta_E + 1) - 1 \quad (3)$$

where  $f$  is the area fraction of the solid/liquid contact area.

Following the Wenzel and Cassie–Baxter equations, the influence of geometric parameters on the apparent contact angle can be understood. PUA coating and TC4 micropillars constitute the superhydrophobic and hydrophilic regions, respectively. Note that PUA coating around micropillars dips slightly and forms curved valleys there (Fig. S4 in the ESM), thus the Cassie–Baxter state holds. When the edge length is constant ( $L = 300 \mu\text{m}$ , Fig. 2(b)), increasing the area ratio  $r$  of PUA coating would enhance this wetting state. When the area ratio is constant ( $r = 75\%$ , Fig. 2(a)), increasing  $L$  of micropillars to  $500 \mu\text{m}$  would increase the hydrophilic region, and liquid tends to wet the valley, thus the apparent contact angle is nearly the same as the untextured superhydrophobic surface.

While for  $L = 100 \mu\text{m}$ , it is estimated that the valleys are too narrow that less PUA coating is cured inside (Fig. S4(a) in the ESM). As a result, the apparent contact angle is even lower than that on the untextured one. Overall, to achieve a combined performance of super-hydrophobicity and slippery (small roll-off angle), micropillars pattern with an edge length ( $L$ ) of  $300 \mu\text{m}$  and an area ratio ( $r$ ) of 64% is recommended.

### 3.2 Mechanical stability

Mechanical stability (wear-resistant) of the prepared surfaces was evaluated via a sandpaper abrasion test (1,200 mesh). As shown in Fig. 3(a), the specimen ( $L = 300 \mu\text{m}$ ,  $r = 85.9\%$ ) is fixed on a PMMA holder in a reciprocating motion (40 cm) under a load of 7 N. Apparent contact and roll-off angles are plotted as a function of the abrasion cycle. Note that the apparent contact angle decreases gradually from 156° to 130° within 70 cycles, and then remains unchanged. The roll-off angle increases very slowly within the initial 40 cycles (<10°), and after 50 cycles, droplets cannot roll off from the surface even tilting it to 90° or upside down (insets).

To determine the mechanism, EDS images of the metal support and the valley positions on the surface are presented in Fig. 3(b) (acceleration voltage of 15.0 kV and take-off angle of 35.0°). Referring to the chemical composition of the PUA coating (Fig. S2(a) in the ESM), it can be confirmed that most PUA on the metal support was removed (Area 2), only with a little residuum. The chemical composition is complex at the valley positions (Area 1), since not only PUA coating, but also worn TC4 particles exist there. It means that wear particles were generated from TC4 pillars within the reciprocating process, and they were inlaid into the PUA coating within the sliding process, as the schematic diagram in Fig. 3(c) indicated. Note that the magnitude of the free surface energy of TC4 ( $\sim 10^3 \text{ mJ/m}^2$ ) is much higher than that of PUA coating ( $\sim 10^1 \text{ mJ/m}^2$ ). The free surface energy is increased with the accumulation of TC4 particles in the curved valley of PUA coating, and the curved valley becomes smooth as the abrasion progresses, thus less air would be trapped inside the valleys. These together yield a decrement of apparent contact

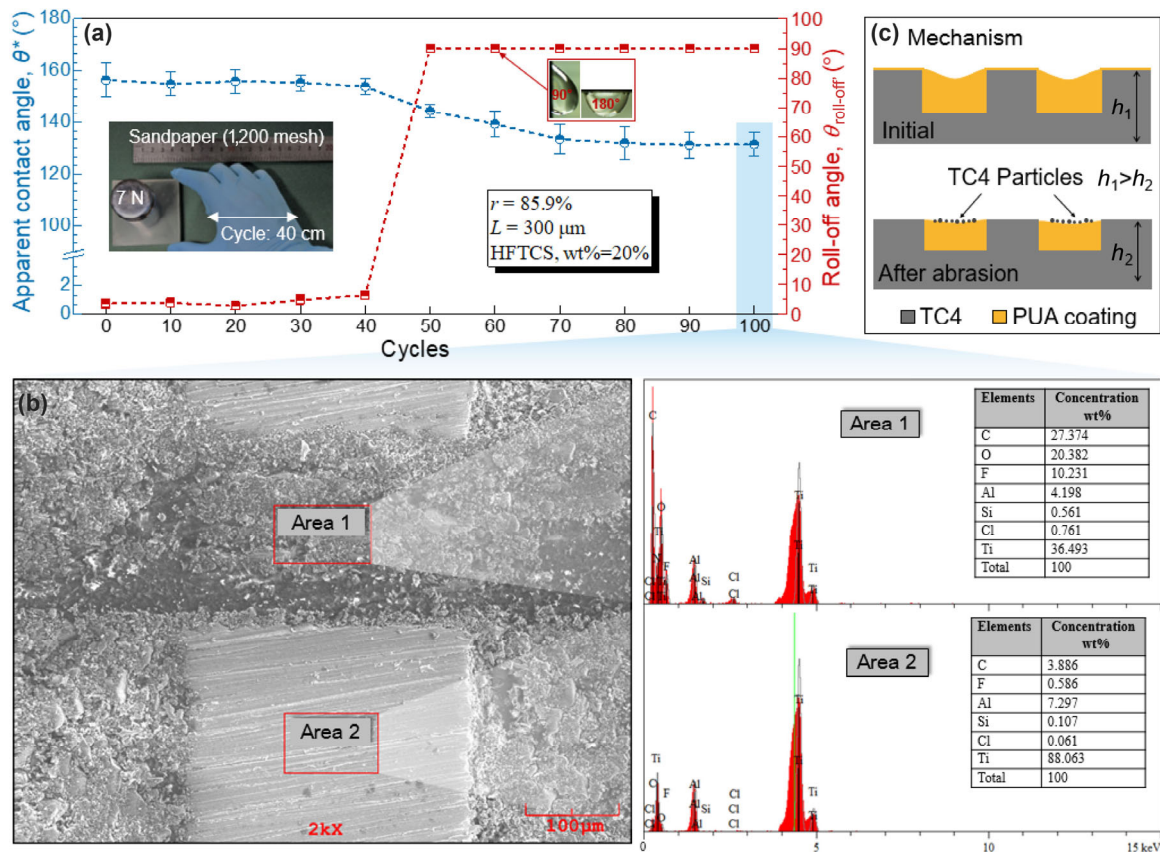


**Fig. 3** Mechanical stability experiments of the prepared surface. (a) Apparent contact angle and roll-off angle on the surface with increasing cycles; (b) EDS images of the metal support and the valley positions on the surface; and (c) schematic diagram of the wear-resistant mechanism.

angle and an increment of roll-off angle with increasing cycles. It is believed that the excellent wear-resistance performance is attributed to the metal supports, and the superhydrophobicity capacity is contributed by the PUA coating.

Figure 4 exhibits the detailed mechanical stability and the microscopic images of all prepared surfaces under a load of 7 N and 100 cycles (each 40 cm). As shown in Figs. 4(a) and 4(a'), on patterned surfaces with a fixed area ratio  $r$  of 75%, when  $L = 100 \mu\text{m}$ , the apparent contact angle is  $110^\circ$ , and it increases to  $135^\circ$  as  $L$  increases to  $500 \mu\text{m}$ . It is because the stress concentration around the micropillars with a larger  $L$  is much lower than that with a smaller  $L$ , the corresponding wear particles would be much less [55]. Referring to Fig. 3(c), less worn particles would have a weaker effect on the degeneration of the superhydrophobicity of the PUA coating. As a result, the apparent contact angle just slightly decreases.

As shown in Figs. 4(b) and 4(b'), on patterned

surfaces with a fixed edge length  $L$  of  $300 \mu\text{m}$ , the apparent contact angle increases from  $95^\circ$  to  $132^\circ$  as the area ratio increases from 43.7% to 85.9%. It is because the stress concentration around the micropillars with a constant  $L$  is nearly the same, thus they have a similar wear-resistant performance. In the meanwhile, as the area ratio exceeds 50%, the PUA coating would have a dominant role, enhancing the superhydrophobicity. Overall, the magnitude of the degeneration of the superhydrophobicity of these prepared surfaces is similar to that reported in Ref. [51]. Micropillars with a larger edge length or PUA coating with a larger area ratio is recommended to achieve a mechanically durable superhydrophobic property.

### 3.3 Droplet impact performance

Figure 5(a) shows the water droplets (diameter of 3.1 mm) impacting process on the fabricated surfaces under different conditions. Four typical impacting

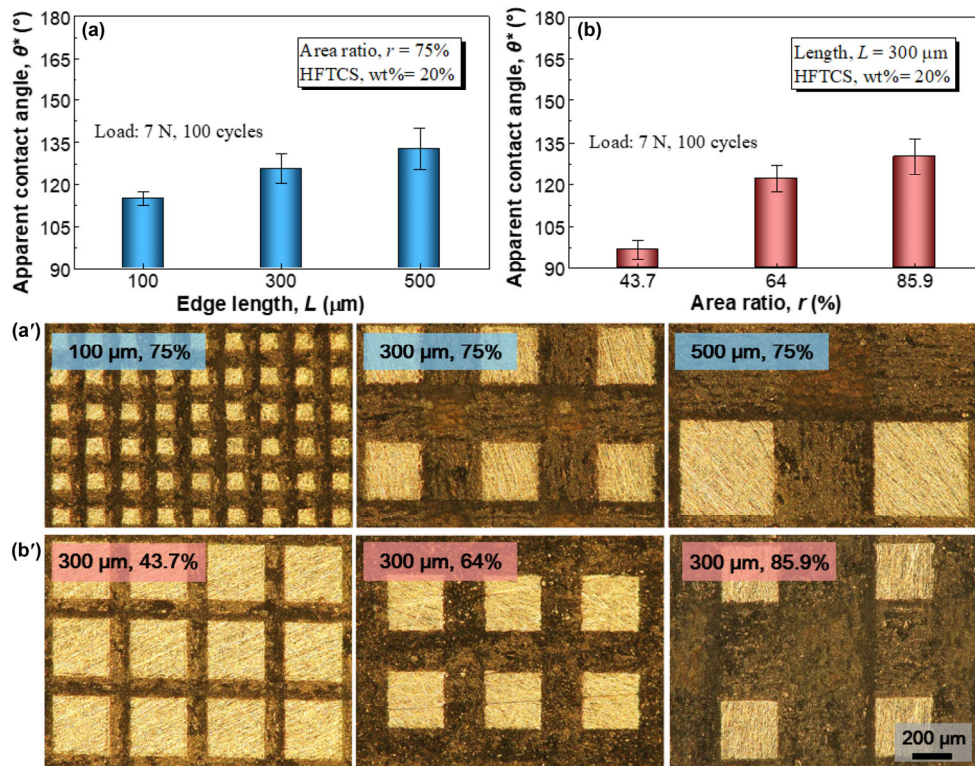


**Fig. 4** Wear resistance performance of the fabricated superhydrophobic surfaces of different parameters under a load of 7 N and 100 cycles (40 cm each): (a) and (a') edge length; (b) and (b') area ratio.

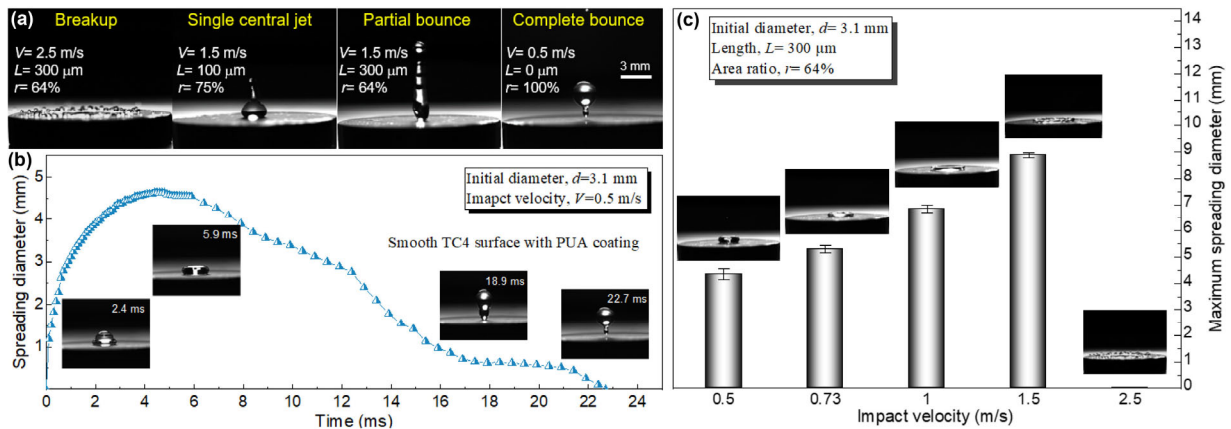


**Fig. 5** (a) Four typical impact phenomena of water droplets on the fabricated surfaces; (b) dynamic impacting and bouncing process of a water droplet on the smooth TC4 surface with PUA coating and the detailed spreading diameter with elapsed time; and (c) influence of impact velocity on the maximum spreading diameter on the structured surface of  $L = 300 \mu\text{m}$  and  $r = 64\%$ .

phenomena of breakup, single central bounce, partial bounce, and complete bounce are observed, which depend on the impact velocity and the surface structure. The detailed impacting and bouncing process on the smooth TC4 surface with PUA coating (fourth panel in Fig. 5(a)), and the corresponding spreading diameter with elapsed time is shown in Fig. 5(b). Droplet undergoes a general process of impacting,

spreading, retracting, and complete bouncing. It spreads to the maximum diameter within 5.9 ms and retracts gradually to the center within 22.7 ms before completely bouncing. The time from retracting to bouncing is nearly three times longer than that of spreading to the maximum diameter. Figure 5(c) shows the influence of impact velocity (diameter of 3.1 mm) on the maximum spreading diameter on the

structured surface of  $L = 300 \mu\text{m}$  and  $r = 64\%$  (details are provided in Fig. S5 in the ESM). It can be seen that the maximum spreading diameter (the diameter before the droplet begins to retract) increases gradually with increasing impact velocity, and it is regarded as zero since the droplet breakup at a velocity of 2.5 m/s. This trend can be understood from the perspective of energy conversion. As the droplet impact progresses, a transformation between kinetic energy, surface energy, and viscous dissipation energy occurs. Note that the roll-off angles are small enough on superhydrophobic surfaces (Fig. 2), thus, the initial kinetic energy mainly transforms into surface energy, resulting in deformation. Droplet deformation is relatively smooth under a low impact velocity, and the intensity becomes strong as the velocity increases. Once the deformation can no longer absorb the initial kinetic energy, droplets would break up into small ones and splash out to consume the excess kinetic energy. For the sake of comparison, a small impact velocity of 0.5 m/s is adopted to evaluate the fabricated surfaces with different parameters.

Figure 6(a) shows the dynamic repelling performances of water droplets on all designed surfaces with a diameter of 3.1 mm and an impact velocity of 0.5 m/s. Since the initial smooth TC4 surface is hydrophilic and the impact velocity is relatively small, the droplet would just impact and spread on it, without any bouncing. Here, the untextured superhydrophobic surface is compared. All droplets bounced in a pancake shape, and the contacting time is dramatically reduced when the surfaces are featured with micropillars. The

spreading time (from contact to max spreading diameter), the contracting time (from max spreading diameter to detachment), and the contacting time (from contact to detachment) are compared in Fig. 6(b). Note that the untextured surface has the longest contacting time ( $\sim 22.7$  ms), for micropillars pattern with a smaller edge length or a larger area ratio, the contact time would be shorter. Patterned surface with  $L = 100 \mu\text{m}$  and  $r = 75\%$  or  $L = 300 \mu\text{m}$  and  $r = 85.9\%$  has a relatively short contacting time of 17.8 and 17.5 ms, respectively; this time decreases nearly 25% compared to that of the untextured one, which is a benefit for enhancing the water resistance performance.

It is known that the surface energy of a droplet ( $E_s$ ) satisfies Eq. (4):

$$E_s \approx \pi \gamma_{LV} D^2 (\cos \theta_{\text{rec}} - \cos \theta_{\text{adv}}) \quad (4)$$

where  $D$  is the droplet diameter,  $\theta_{\text{rec}}$  and  $\theta_{\text{adv}}$  are the receding and advancing contact angle, respectively.

The initial kinetic energy of a droplet ( $E_k$ ) can be estimated by [56]:

$$E_k \approx \frac{1}{12} \pi \rho D^3 V^2 \quad (5)$$

where  $\rho$  is the density and  $V$  is the impacting velocity.

For the surface deformation to accommodate the kinetic energy, the order of magnitude of  $E_s$  and  $E_k$  should be the same. For the tested water droplets ( $\gamma_{LV} = 72 \text{ mN}\cdot\text{m}^{-1}$ ,  $\rho = 1,000 \text{ kg}\cdot\text{m}^{-3}$ ,  $D = 3.1 \text{ mm}$ ,  $\theta_{\text{rec}} = \sim 2^\circ$ ,  $\theta_{\text{adv}} = \sim 160^\circ$ ), the corresponding impact velocity

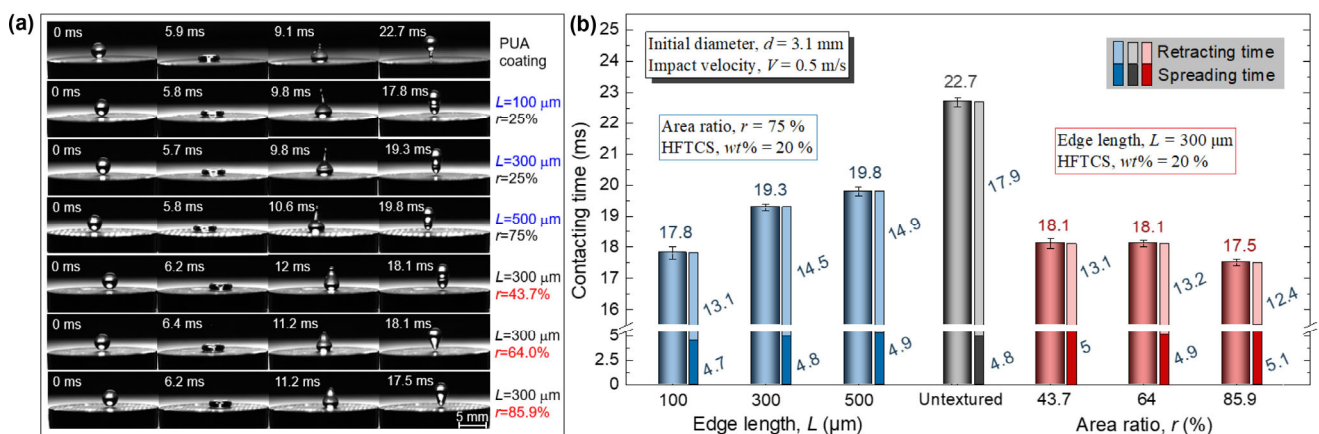


**Fig. 6** Droplet impact performance of the prepared superhydrophobic surfaces. Dynamic process with (a) elapsed time and (b) contacting time.

should be no less than 0.2 m/s. In this study, all water droplets can bounce since the experimental impacting velocities are higher than 0.5 m/s. The ratio of the kinetic and surface energies can also be characterized by the nondimensional Weber number ( $\frac{\rho V^2 D}{\gamma_{LV}}$ ). For

all droplets under consideration, the order of magnitude of Weber number is 10, which is high enough for bouncing.

### 3.4 Anti-frosting performance

Figure 7 present an intuitive comparison between the frosting process on the smooth and patterned ( $L = 300 \mu\text{m}$ ,  $r = 85.9\%$ ) surfaces within 6 min. Seeing from the side view in Fig. 7(a), an obvious difference occurs after 4 min, that is, much more water frosts on the smooth TC4 surface than that on the patterned one, and the final frost layer thickness on the smooth surface are much thicker. As the grid's eye view in

Fig. 7(c) indicates, a large area of frost is generated on the smooth surface, while the frost is sporadically generated on the patterned surface.

The frost mass on these fabricated surfaces within 6 min is measured and shown in Fig. 7(b). Compared to the smooth TC4 surface, most fabricated superhydrophobic surfaces have an excellent anti-frosting performance, except the surface with  $L = 500 \mu\text{m}$  and  $r = 75\%$ . Note that decreasing the edge length  $L$  (blue histogram) or increasing the area ratio  $r$  (red histogram) would enhance the anti-frosting performance. On the surface with a pattern of  $L = 100 \mu\text{m}$  and  $r = 75\%$  or  $L = 300 \mu\text{m}$  and  $r = 85.9\%$ , the frost mass is reduced by 50% more than that on the untreated one. It is confirmed that the fabricated superhydrophobic surface has an excellent anti-frosting performance, and some reported work indicates that superhydrophobic treatment on steel surfaces could increase the frozen time to approximately 50% or less [57, 58].

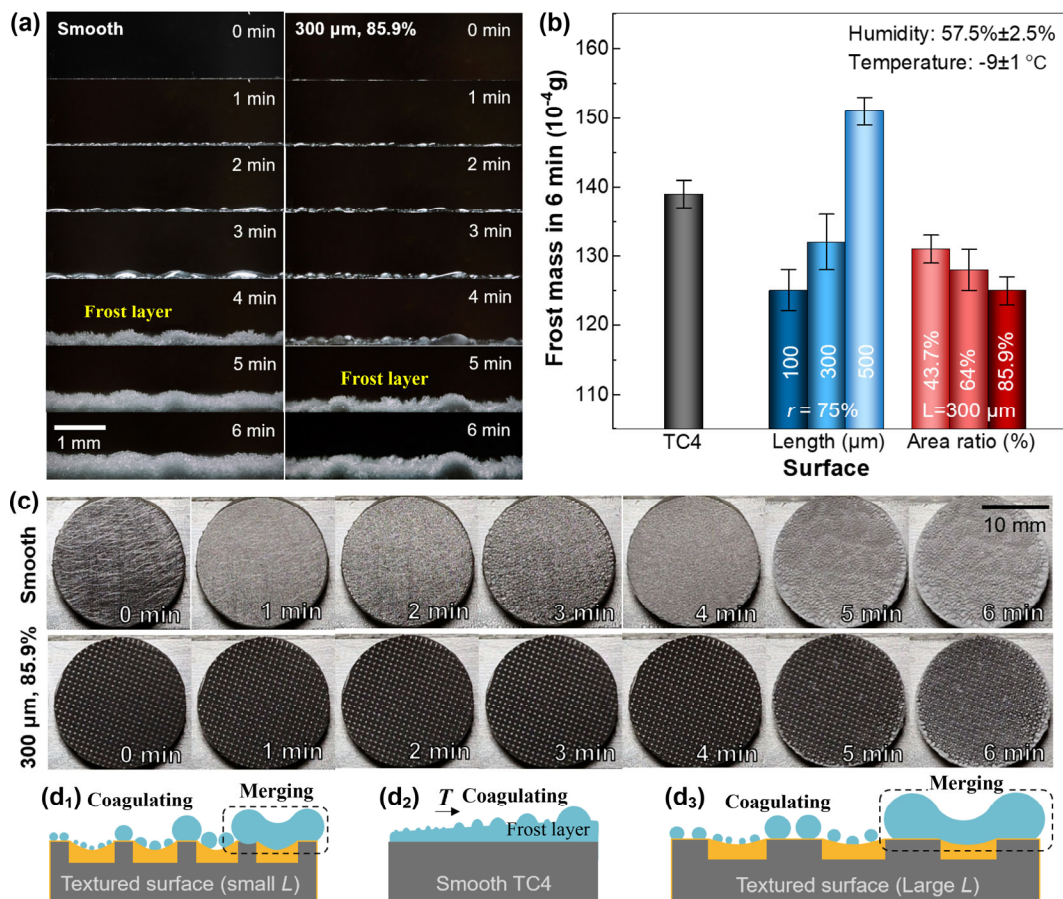


**Fig. 7** Frost resistance phenomena of the smooth TC4 surface and the fabricated surface ( $L = 300 \mu\text{m}$ ,  $r = 85.9\%$ ) within 6 min. (a) Side view; (b) frost resistance performances of all fabricated surfaces; (c) bird's eye view; and (d) mechanism.

The anti-frosting mechanism is explained as follows. As shown in Fig. 7(d<sub>2</sub>), vaporous water gradually coagulates on the smooth TC4 surface; as time elapses, a frost layer is formed on the TC4 surface associated with micro frost needles on the top (seeing from the fourth panel in Fig. 7(a)), this frost layer would hinder the frosting process to some extent. As shown in Fig. 7(d<sub>1</sub>), when TC4 surfaces are decorated with micropillars of a small edge length  $L$  or a large area density, PUA coating would slow down the coagulation progress, exhibiting an anti-frosting capacity; as time elapses, droplets would merge on the conjoint pillars, resulting in a degradation of anti-frosting capacity, while it is still better than the smooth one. Differently, for micropillars with a large edge length ( $L = 500\text{ }\mu\text{m}$ ), large water droplets coagulate and merge between conjoint pillars; besides, frost layers can hardly generate on the surface. As a result, the frosting process is enhanced.

### 3.5 Further discussion and outlook

Overall, it is confirmed that the fabricated surfaces are with robust superhydrophobicity, wear-resistant, controllable droplet impact, and anti-frosting performances. These characteristics have promising prospects in many applications. Metal support is the key factor for enhancing the anti-wear performance and PUA coating with a larger area ratio contributes to the superhydrophobicity. Parameter optimization of the micropillars pattern is suggested to enhance the anti-resistant capacity for the potential application. For controllable droplet impact and anti-frosting performances, it is confirmed that a small edge length or a larger area ratio would yield a shorter contacting time (Fig. 6(b)) and a smaller frost mass (Fig. 7(b)). The trend is in accordance with the trend of apparent contact angle on these surfaces, although some small fluctuations exist. Generally, it is believed that enhancing the superhydrophobicity would contribute to a shorter droplet impact time and excellent anti-frosting performance.

Although TC4 was used as the basic material in this work, its dominant role is providing shelter for the superhydrophobic PUA coating. It can be determined that this fabrication method is suitable

for most metal materials. As we know, laser etching is of high efficiency compared to traditional electron or ion-beam lithographic methods in fabricating micro structures [59]. For the fabricated surface textures with dimensions of 100–500  $\mu\text{m}$  in this study, the mean processing efficiency of nanosecond laser etching (laser power of 3 W) and PUA coating (ultraviolet light power of 400 W) is approximately 15 and 100  $\text{mm}^2/\text{min}$ , respectively. Combining laser etching and PUA coating to achieve high-performance robust superhydrophobic surfaces is of significant advantage, which would be suitable for rapid large-scale surface manufacturing in the future with the rational use of industrial-grade high power laser and ultraviolet light.

## 4 Conclusions

In this work, we proposed a feasible method to fabricate robust superhydrophobic surfaces. Polyurethane acrylate (PUA) coating with 20 wt% or higher 1H,1H,2H,2H-Perfluorodecyltrichlorosilane (HFTCS) content is of excellent superhydrophobic capacity. Via fabricating micropillars pattern on titanium alloy (TC4) surfaces and curing PUA coating in the valleys around the pattern, robust superhydrophobicity is achieved, of which metal micropillars pattern and PUA coating provide wear-resistant and superhydrophobicity, respectively. The apparent contact angle on fabricated surfaces could reach  $167^\circ$ . Micropillars pattern with a larger edge length or PUA coating with a larger area ratio is suggested to achieve a mechanically durable superhydrophobic property. The parameter of  $L = 300\text{ }\mu\text{m}$  and  $r = 85.9\%$  is highly recommended to achieve excellent droplet impacting and anti-frosting performances. The proposed design principle is of potential applications to improve the performance of traditional mechanical systems.

## Acknowledgements

The authors are grateful for the support provided by the National Natural Science Foundation of China (No. 51805252), the Tribology Science Fund of State Key Laboratory of Tribology (No. SKLTKF21B02), and the Alexander von Humboldt Foundation.

## Declaration of competing interest

The authors have no competing interests to declare that are relevant to the content of this article.

**Electronic Supplementary Material:** Supplementary material is available in the online version of this article at <https://doi.org/10.1007/s40544-023-0757-3>.

**Open Access** This article is licensed under a Creative Commons Attribution 4.0 International License, which permits use, sharing, adaptation, distribution and reproduction in any medium or format, as long as you give appropriate credit to the original author(s) and the source, provide a link to the Creative Commons licence, and indicate if changes were made.

The images or other third party material in this article are included in the article's Creative Commons licence, unless indicated otherwise in a credit line to the material. If material is not included in the article's Creative Commons licence and your intended use is not permitted by statutory regulation or exceeds the permitted use, you will need to obtain permission directly from the copyright holder.

To view a copy of this licence, visit <http://creativecommons.org/licenses/by/4.0/>.

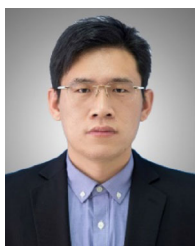
## References

- [1] Young T. An essay on the cohesion of fluids. *Phil Trans R Soc Lond* **95**: 65–87 (1805)
- [2] Lv C J, Hao P F. Driving droplet by scale effect on microstructured hydrophobic surfaces. *Langmuir* **28**(49): 16958–16965 (2012)
- [3] Chen H W, Zhang P F, Zhang L W, Liu H L, Jiang Y, Zhang D Y, Han Z W, Jiang L. Continuous directional water transport on the peristome surface of *Nepenthes alata*. *Nature* **532**(7597): 85–89 (2016)
- [4] Grützmacher P G, Rosenkranz A, Szurdak A, Gachot C, Hirt G, Mücklich F. Lubricant migration on stainless steel induced by bio-inspired multi-scale surface patterns. *Mater Design* **150**: 55–63 (2018)
- [5] Yan X T, Jin Y K, Chen X M, Zhang C, Hao C L, Wang Z W. Nature-inspired surface topography: design and function. *Sci China Phys Mech* **63**(2): 224601 (2019)
- [6] Jing X, Guo Z. Durable lubricant-impregnated surfaces for water collection under extremely severe working conditions. *ACS Appl Mater Inter* **11**(39): 35949–35958 (2019)
- [7] Dai Q W, Huang W, Wang X L, Khonsari M M. Directional interfacial motion of liquids: Fundamentals, evaluations, and manipulation strategies. *Tribol Int* **154**: 106749 (2021)
- [8] Tang Y, Yang X L, Li Y M, Lu Y, Zhu D. Robust micro-nanostructured superhydrophobic surfaces for long-term dropwise condensation. *Nano Lett* **21**(22): 9824–9833 (2021)
- [9] Xu Q, Wan Y, Hu T S, Liu T X, Tao D, Niewiarowski P H, Tian Y, Liu Y, Dai L, Yang Y, Xia Z. Robust self-cleaning and micromanipulation capabilities of gecko spatulae and their bio-mimics. *Nat Commun* **6**: 1–9 (2015)
- [10] Lu Y, Sathasivam S, Song J, Crick C R, Carmalt C J, Parkin I P. Robust self-cleaning surfaces that function when exposed to either air or oil. *Science* **347**(6226): 1132–1135 (2015)
- [11] Yong J, Chen F, Yang Q, Huo J, Houa X. Superoleophobic surfaces. *Chem Soc Rev* **46**(14): 4168–4217 (2017)
- [12] Yang X L, Song J L, Zheng H L, Deng X, Liu X, Lu X H, Sun J, Zhao D Y. Anisotropic sliding on dual-rail hydrophilic tracks. *Lab on a Chip* **17**(6): 1041–1050 (2017)
- [13] Celia E, Darmanin T, Givenchy E T D, Amigoni S, Guittard F. Recent advances in designing superhydrophobic surfaces. *J Colloid Interf Sci* **402**: 1–18 (2013)
- [14] Rahman M A, Jacobi A M. Experimental study on frosting/defrosting characteristics of microgrooved metal surfaces. *Int J Refrig* **50**: 44–56 (2015)
- [15] Wang N, Xiong D, Lu Y, Pan S, Wang K, Deng Y, Shi Y. Design and fabrication of the lyophobic slippery surface and its application in anti-icing. *J Phys Chem C* **120**(20): 11054–11059 (2016)
- [16] Yang X, Breedveld V, Choi W T, Liu X, Song J, Hess D W. Underwater curvature-driven transport between oil droplets on patterned substrates. *ACS Appl Mater Interfaces* **10**(17): 15258–15269 (2018)
- [17] Si Y, Dong Z. Bioinspired smart liquid directional transport control. *Langmuir* **36**(3): 667–681 (2020)
- [18] Yang X L, Zhuang K, Lu Y, Wang X L. Creation of topological ultraslippery surfaces for droplet motion control. *ACS Nano* **15**(2): 2589–2599 (2021)
- [19] Cheng J, Wang G, Zhang Y, Pi P, Xu S. Enhancement of capillary and thermal performance of grooved copper heat pipe by gradient wettability surface. *Int J Heat Mass Tran* **107**: 586–591 (2017)
- [20] Zhang X Y, Huang M Y, Ji Q, Luo X B. Lattice Boltzmann modeling and experimental study of water droplet spreading on wedge-shaped pattern surface. *Int J Heat Mass Tran* **130**: 857–861 (2019)
- [21] Dai Q W, Chen S Q, Huang W, Wang X L, Hardt S. On the thermocapillary migration between parallel plates. *Int J Heat Mass Tran* **182**: 121962 (2022)

- [22] Ta V D, Dunn A, Wasley T J, Li J, Kay R W, Stringer J, Smith P J, Esenturk E, Connaughton C, Shephard J D. Laser textured surface gradients. *Appl Surf Sci* **371**: 583–589 (2016)
- [23] Dai Q W, Ji Y J, Chong Z J, Huang W, Wang X L. Manipulating thermocapillary migration via superoleophobic surfaces with wedge shaped superoleophilic grooves. *J Colloid Interf Sci* **557**: 837–844 (2019)
- [24] Sommers A D, Panth M, Eid K F. Self-propelled water droplet movement on a laser-etched radial gradient copper surface. *Appl Therm Eng* **173**: 115226 (2020)
- [25] Bai X, Yang Q, Fang Y, Zhang J, Yong J, Hou X, Chen F. Superhydrophobicity-memory surfaces prepared by a femtosecond laser. *Chem Eng J* **383**: 123143 (2020)
- [26] Morgenthaler S, Zink C, Spencer N D. Surface-chemical and -morphological gradients. *Soft Matter* **4**(3): 419–434 (2008)
- [27] Zhang C, McAdams D A, Grunlan J C. Nano/micro-manufacturing of bioinspired materials: A review of methods to mimic natural structures. *Adv Mater* **28**(30): 6292–6321 (2016)
- [28] Yao C W, Tang S, Sebastian D, Tadmor R. Sliding of water droplets on micropillar-structured superhydrophobic surfaces. *Appl Surf Sci* **504**: 144493 (2020)
- [29] Riau A K, Mondal D, Setiawan M, Palaniappan A, Yam G H, Liedberg B, Venkatraman S S, Mehta J S. Functionalization of the polymeric surface with bioceramic nanoparticles via a novel, nonthermal dip coating method. *ACS Appl Mater Interfaces* **8**(51): 35565–35577 (2016)
- [30] Pradheebha S, Unnikannan R, Bathe R N, Padmanabham G, Subasri R. Effect of plasma pretreatment on durability of sol-gel superhydrophobic coatings on laser modified stainless steel substrates. *J Adhes Sci Technol* **32**(21): 2394–2404 (2018)
- [31] Faustini M, Ceratti D R, Louis B, Boudot M, Albouy P A, Boissière C, Grosso D. Engineering functionality gradients by dip coating process in acceleration mode. *ACS Appl Mater Inter* **6**(19): 17102–17110 (2014)
- [32] Karapanagiotis I, Manoudis P N, Zurba A, Lampakis D. From hydrophobic to superhydrophobic and superhydrophilic siloxanes by thermal treatment. *Langmuir* **30**(44): 13235–13243 (2014)
- [33] Gao L, McCarthy T J. How wenzel and cassie were wrong. *Langmuir* **23**: 3762–3765 (2007)
- [34] Extrand C W. Origins of wetting. *Langmuir* **32**(31): 7697–7706 (2016)
- [35] Parvate S, Dixit P, Chattopadhyay S. Superhydrophobic surfaces: Insights from theory and experiment. *J Phys Chem B* **124**(8): 1323–1360 (2020)
- [36] Bormashenko E. Progress in understanding wetting transitions on rough surfaces. *Adv Colloid Interface Sci* **222**: 92–103 (2015)
- [37] Yamamoto M, Nishikawa N, Mayama H, Nonomura Y, Yokojima S, Nakamura S, Uchida K. Theoretical explanation of the lotus effect: Superhydrophobic property changes by removal of nanostructures from the surface of a lotus leaf. *Langmuir* **31**(26): 7355–7363 (2015)
- [38] Ren W. Wetting transition on patterned surfaces: Transition states and energy barriers. *Langmuir* **30**(10): 2879–2885 (2014)
- [39] Grynyov R, Bormashenko E, Whyman G, Bormashenko Y, Musin A, Pogreb R, Starostin A, Valtsifer V, Strelnikov V, Schechter A, Kolagatla S. Superoleophobic surfaces obtained via hierarchical metallic meshes. *Langmuir* **32**(17): 4134–4140 (2016)
- [40] Lambley H, Schutzius T M, Poulikakos D. Superhydrophobic surfaces for extreme environmental conditions. *Proc Natl Acad Sci* **117**(44): 27188–27194 (2020)
- [41] Liu T, Kim C J. Turning a surface superrepellent even to completely wetting liquids. *Science* **346**: 1096–1099 (2014)
- [42] Löblein S M, Mücklich F, Grützmacher P G. Topography versus chemistry—How can we control surface wetting? *J Colloid Interf Sci* **609**: 645–656 (2022)
- [43] Liu M J, Wang S T, Jiang L. Nature-inspired superwettability systems. *Nat Rev Mater* **2**(7): 17036 (2017)
- [44] Kita Y, Mackenzie Dover C, Askounis A, Takata Y, Sefiane K. Drop mobility on superhydrophobic microstructured surfaces with wettability contrasts. *Soft Matter* **14**(46): 9418–9424 (2018)
- [45] Liu C, Zhan H, Yu J, Liu R, Zhang Q, Liu Y, Li X. Design of superhydrophobic pillars with robustness. *Surf Coat Technol* **361**: 342–348 (2019)
- [46] Torun I, Onses M S. Robust superhydrophobicity on paper: Protection of spray-coated nanoparticles against mechanical wear by the microstructure of paper. *Surf Coat Technol* **319**: 301–308 (2017)
- [47] Xie J, Hu J, Lin X, Fang L, Wu F, Liao X, Luo H, Shi L. Robust and anti-corrosive PDMS/SiO<sub>2</sub> superhydrophobic coatings fabricated on magnesium alloys with different-sized SiO<sub>2</sub> nanoparticles. *Appl Surf Sci* **457**: 870–880 (2018)
- [48] Han X, Peng J, Jiang S, Xiong J, Song Y, Gong X. Robust superamphiphobic coatings based on raspberry-like hollow SnO<sub>2</sub> composites. *Langmuir* **36**(37): 11044–11053 (2020)
- [49] Zhang B, Xu W, Xia D, Huang Y, Zhao X, Zhang J. Spray coated superamphiphobic surface with hot water repellency and durable corrosion resistance. *Colloids Surf A* **596**: 124750 (2020)

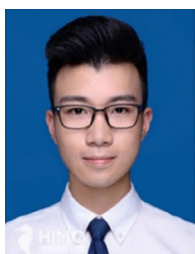


- [50] Li H, Zhu G, Shen Y, Han Z, Zhang J, Li J. Robust superhydrophobic attapulgite meshes for effective separation of water-in-oil emulsions. *J Colloid Interface Sci* **557**: 84–93 (2019)
- [51] Wang D H, Sun Q Q, Hokkanen M J, Zhang C L, Lin F Y, Liu Q, Zhu S P, Zhou T, Chang Q, He B, Zhou Q, Chen L, Wang Z, Ras R H A, Deng X. Design of robust superhydrophobic surfaces. *Nature* **582**(7810): 55–59 (2020)
- [52] Chen S Q, Dai Q W, Yang X L, Liu J J, Huang W, Wang X L. Bioinspired functional structures for lubricant control at surfaces and interfaces: Wedged-groove with oriented capillary patterns. *ACS Appl Mater Inter* **14**: 42635–42644 (2022)
- [53] Xu M, Sun G, Kim C J. Infinite lifetime of underwater superhydrophobic states. *Phys Rev Lett* **113**(13): 136103 (2014)
- [54] Tadmor R. Approaches in wetting phenomena. *Soft Matter* **7**(5): 1577–1580 (2011)
- [55] Wang X L, Wang J Q, Zhang B, Huang W. Design principles for the area density of dimple patterns. *Proc Inst Mech Eng Part J* **229**: 538–546 (2015)
- [56] Nosonovsky M, Bhushan B. Energy transitions in superhydrophobicity: Low adhesion, easy flow and bouncing. *J Phys Condens Matter* **20**(39): 395005 (2008)
- [57] Chen T, Yan W, Hongtao L, Zhu W, Guo K, Li J. Facile preparation of superamphiphobic phosphate–Cu coating on iron substrate with mechanical stability, anti-frosting properties, and corrosion resistance. *J Mater Sci* **52**(8): 4675–4688 (2017)
- [58] Ma Q, Wang W, Dong G. Facile fabrication of biomimetic liquid-infused slippery surface on carbon steel and its self-cleaning, anti-corrosion, anti-frosting and tribological properties. *Colloids Surf A* **577**: 17–26 (2019)
- [59] Lasagni A, Benke D, Kunze T, Bieda M, Eckhardt S, Roch T, Langheinrich D, Berger J. Bringing the direct laser interference patterning method to industry: A one tool-complete solution for surface functionalization. *J Laser Micro/Nanoeng* **10**(3): 340–344 (2015)



**Qingwen DAI.** He received his B.Eng. and Ph.D. degrees in mechanical engineering from Nanjing University of Aeronautics & Astronautics, China, in 2011 and 2017, respectively. He was awarded

as a Humboldt Research Fellow, Germany, in 2021. His current position is an associate professor at Nanjing University of Aeronautics & Astronautics. His research areas cover surface texturing, lubrication migration control, and microfluidics.



**Lei CHEN.** He received his B.Eng. degree in mechanical engineering from Shanghai Maritime University, China, in 2018. Then, he became a

master student at Nanjing University of Aeronautics & Astronautics, China, in 2019. His research interest is lubricant impact and migration on textured surfaces.



**Dameng LIU.** He received his Ph.D. degree from University of Cambridge, UK. He is an associate professor and a doctoral supervisor at Tsinghua University, China. In the last couple of years, his main

research interests include friction energy dissipation mechanism, photoelectric nondestructive testing technology, composite testing equipment, and flexible material manufacturing equipment. He has authored over 70 SCI papers, including *Advanced Materials*, *ACS Nano*, *Nano Letters*, and other high-impact journals.



**Wei HUANG.** He received his Ph.D. degree in material science from Central Iron & Steel Research Institute, China, in 2008. His

current position is a professor at Nanjing University of Aeronautics and Astronautics, China. His research areas cover magnetic fluid, friction reduction, and anti-wear coating design.



**Xiaolei WANG.** He received his Ph.D. degree in mechanical engineering from Tohoku University, Japan, in 2001. His current position is a professor at Nanjing

University of Aeronautics and Astronautics, China. His research areas cover surface texturing, bioinspired fabrication, mechanical seal, bearing, coatings, and lubrication under special working conditions.